Article

Determination of Steady-State and Faulty Regimes of Overhead Lines by Means of Multiconductor Cell Analysis (MCA)

Roberto Benato *, Sebastian Dambone Sessa and Fabio Guglielmi

Department of Industrial Engineering, University of Padova, Via Gradenigo, 6/A, Padova 35131, Italy;
E-Mails: sebastian.dambonesessa@unipd.it (S.D.S.); fabio.guglielmi@unipd.it (F.G.)

* Author to whom correspondence should be addressed; E-Mail: roberto.benato@unipd.it;
Tel.: +39-049-827-7532; Fax: +39-049-827-7599.

Abstract: Single-phase positive sequence modelling is often used in power systems when power flows and short circuit analysis are assessed. Of course, the use of single-phase positive sequence modelling assumes purely three-phase configurations and perfectly symmetrical ones so that single-phase modelling considers that all the phase conductors behave in the same way. When considering the physical reality of power networks, this assumption can be questionable and the behaviors of all the system conductors including the passive ones (earth wires for overhead lines, metallic screens and armours for cables and enclosures for gas insulated lines) is completely unknown. Therefore, the present multiconductor cell analysis (MCA) becomes necessary, since it allows one to achieve great precision results on the regimes of both phase conductors and passive conductors. MCA offers a powerful tool in order to validate (or less) approximated and simplified computation methods. In particular, for single and double circuit overhead lines (OHLs), the current phasors induced in the earth wires and the ground return current alongside the line can be directly computed by MCA in steady state and faulty regimes. It is worth noting that, for faulty regimes, MCA allows also evaluating the approximation degree and validity field of screening factors k.

1. Introduction

Multiconductor cell analysis (MCA) takes advantage of the extensive use of the admittance matrices in order to consider any asymmetrical system with all the active and passive (earth wires for OHLs, screens and armors for underground insulated cables (UGCs), enclosures for gas insulated lines (GILs), keraunic wires, buried conductors, rails, feeders, overhead contact line with catenary suspension for AC high speed railway systems) conductors. It allows knowing directly the electrical behaviors of all the electrical quantities alongside an OHL. In the following, the steady state regime and the faulty regime of OHLs are considered. Furthermore a comparison between MCA and the commercial software EMTP-RV results is presented, which has given a very good agreement.
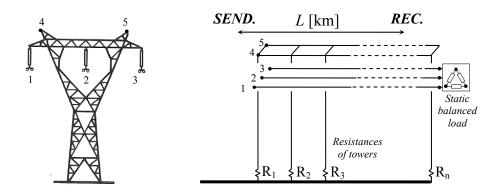
2. Application of MCA to Overhead Lines

MCA has been already applied to a great number of asymmetrical systems: cross-bonded underground insulated cables [1,2], shunt compensated ones, distribution line carrier, solid bonded or multiple-point bonded gas insulated lines [3], Milliken type EHV insulated cables. In this paper a thorough exposition of the application of MCA to overhead lines is presented. It allows considering:

(1) Single or double circuit in electrical parallel with any type of phasing (low reactance or super bundle ones);
(2) Any tower type, with different earth resistivities along the line and different tower resistances;
(3) The steady-state regime of an OHL supplying a balanced (or not) three-phase load;
(4) Faulty regimes (line-to-earth, line-to-line, line-to-line-to-earth, three phase short-circuit), with two end substations each characterized by its own fault levels.

For the sake of a clear explanation, let us consider a single-circuit OHL composed of five conductors ($n = 5$; see Figure 1) parallel to themselves and to the ground: 1, 2, 3 are the phase conductors (in Figure 1, bundle ones) and 4, 5 are the earth wires.

Figure 1. Multiconductor representation of OHL supplying a static balanced load; SEND—sending-end; REC—receiving-end.

This multiconductor line may be represented as a cascade of *N* elementary cells of length Δ (e.g., Δ = span length), modelled by a lumped π circuit (see Figure 2).
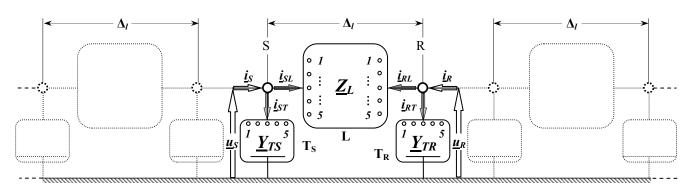
Figure 2. Cascade of *N* elementary cells for OHL modelling.

Being Δ sufficiently small, it is possible to lump distributed shunt admittances at the ends of the cell ($\underline{Y}_{TS}$ and $\underline{Y}_{TR}$ are the transverse blocks), thus allowing the separate study of longitudinal elements. In order to form $\underline{Z}_L$, it is necessary to compute the self and mutual longitudinal impedances, which account for the earth return currents. They can be obtained by applying the simplified Carson-Clem formulae [4] or the complete Carson formulae [5] with Carson's corrections in terms of series [6]. It has been widely demonstrated by one of the authors that at power frequency (50 or 60 Hz) the Carson-Clem formulae are very precise and consequently they are a powerful tool so giving the same results of complete Carson ones (Section 5).

In order to give the above mentioned sentence a theoretical justification, the simplified Carson-Clem formulae can be licitly applied if the spacing between conductors $d_{i,j} \leq 0.135D_e$ when $D_e = 658 \cdot \sqrt{\rho/f}$ [m] "Carson Depth"; ρ = electrical resistivity of the soil [Ωm]; f = power frequency (50–60 Hz). By supposing f = 50 Hz and a low earth resistivity e.g., 10 Ωm, it yields:

$$D_e = 658\sqrt{\frac{\rho}{f}} = 658\sqrt{\frac{10}{50}} = 294 \ [\text{m}] \tag{1}$$

The spacings between phases in OHL are never greater than 40 m, therefore it is rather unlikely to have the condition $d_{i,j} > 0.135D_e \cong 40$ m even with very low resistive earth; hence the Carson-Clem formulae can be always used. With great mutual spacings between phases belonging to different circuits in the same corridor, the complete Carson formulae must be used. The self and mutual impedances by means of Carson-Clem formulae are given by:

$$\underline{z}_{i,i} = r_i + \pi^2 \cdot 10^{-4} \cdot f + j4\pi \cdot 10^{-4} \cdot f \cdot \ln\left(\frac{2 \cdot D_e}{d_i'}\right) \ [\Omega/\text{km}] \tag{2}$$

$$\underline{z}_{i,j} = \pi^2 \cdot 10^{-4} \cdot f + j4\pi \cdot 10^{-4} \cdot f \cdot \ln\left(\frac{D_e}{d_{i,j}}\right) \ [\Omega/\text{km}] \tag{3}$$

where r_i = kilometric resistance of conductor i [Ω/km] (if bundle conductor with n subconductors per phase $r_i = r_{i\_sub}/n$); $d_i' = 2 \cdot \text{GMR} = k''d$ [m] (GMR = Geometrical Mean Radius) where k'' are listed in tables depending upon the composition of the conductor and d [m] is the diameter of the conductor (if bundle conductor:

$$d_i' = 2 \cdot \sqrt[n]{n \cdot k'' \cdot \frac{d_{sub}}{2} \cdot R_{circle}^{n-1}}$$

where R_{circle} [m] is the radius of the circle on which the subconductors lay and d_{sub} [m] is the diameter of the subconductors); $d_{i,j}$ = distance between conductor i and j [m]. Once $\underline{z}_{i,i}$ and $\underline{z}_{i,j}$ have been computed, it is possible to form the matrix $\underline{\mathbf{Z}}_L$ (5 × 5) and to characterize, by means of Equation (4) the steady state regime of longitudinal block **L** of Figure 2 (where all voltage and current vectors are shown):

$$\underline{\mathbf{u}}_S - \underline{\mathbf{u}}_R = \underline{\mathbf{Z}}_L \underline{\mathbf{i}}_{SL} \tag{4}$$

and by considering the evident relation Equation (5):

$$\underline{\mathbf{i}}_{SL} = -\underline{\mathbf{i}}_{RL} \tag{5}$$

it yields:

$$\underline{\mathbf{Z}}_L^{-1} \underline{\mathbf{u}}_S - \underline{\mathbf{Z}}_L^{-1} \underline{\mathbf{u}}_R = \underline{\mathbf{i}}_{SL} \tag{6}$$

$$-\underline{\mathbf{Z}}_L^{-1} \underline{\mathbf{u}}_S + \underline{\mathbf{Z}}_L^{-1} \underline{\mathbf{u}}_R = \underline{\mathbf{i}}_{RL} \tag{7}$$

The Equations (6,7) can be written in an elegant matrix form as:

$$
\underbrace{\begin{array}{|c|}
\hline
\underline{\mathbf{i}}_{SL} \\
\hline
\underline{\mathbf{i}}_{RL} \\
\hline
\end{array}}_{\underline{\mathbf{i}}_{L\Delta}}
=
\underbrace{\begin{array}{|c|c|}
\hline
\underline{\mathbf{Z}}_L^{-1} & -\underline{\mathbf{Z}}_L^{-1} \\
\hline
-\underline{\mathbf{Z}}_L^{-1} & \underline{\mathbf{Z}}_L^{-1} \\
\hline
\end{array}}_{\underline{\mathbf{Y}}_{L\Delta}}
\underbrace{\begin{array}{|c|}
\hline
\underline{\mathbf{u}}_S \\
\hline
\underline{\mathbf{u}}_R \\
\hline
\end{array}}_{\underline{\mathbf{u}}_{\Delta}}
\tag{8}
$$
$$(2n \times 2n)$$

The matrix $\underline{\mathbf{Y}}_{L\Delta}$ (10 × 10) is the admittance matrix regarding block **L** circuit formed by five longitudinal links.

The shunt capacitive matrix computation can be obtained from Maxwell potential coefficient matrix. Its elements are easy to compute from the tower geometry and from the conductor radii [7]. It is worth remembering that the average heights of conductors can be used by means of Equation (9):

$$h_{average} = h_{tower} - \frac{2}{3} \cdot sag \quad [m] \tag{9}$$

where h_{tower} is the conductor height at tower.

Then, as already mentioned, the shunt capacitive and conductive links are divided into two halves and lumped at the ends of the elementary cell. The capacitive susceptances (of half cell) between each conductor are considered in the (5 × 5) matrix $\underline{\mathbf{Y}}_{TS} = \underline{\mathbf{Y}}_{TR}$. The vectors of the shunt currents at both ends of the cell are (see Figure 2):

$$
\underbrace{\begin{array}{|c|}
\hline
\underline{\mathbf{i}}_{ST} \\
\hline
\underline{\mathbf{i}}_{RT} \\
\hline
\end{array}}_{\underline{\mathbf{i}}_{T\Delta}}
=
\underbrace{\begin{array}{|c|c|}
\hline
\underline{\mathbf{Y}}_{TS} & \\
\hline
& \underline{\mathbf{Y}}_{TR} \\
\hline
\end{array}}_{\underline{\mathbf{Y}}_{T\Delta}}
\underbrace{\begin{array}{|c|}
\hline
\underline{\mathbf{u}}_S \\
\hline
\underline{\mathbf{u}}_R \\
\hline
\end{array}}_{\underline{\mathbf{u}}_{\Delta}}
\tag{10}
$$
$$(2n \times 2n)$$

Hence the steady state regime of the elementary cell is represented by $\underline{Y}_\Lambda$ which is the superimposition of $\underline{Y}_{L\Lambda}$ and $\underline{Y}_{T\Lambda}$:

$$
\begin{array}{c}
\left[\dfrac{\underline{i}_S}{\underline{i}_R}\right] = \left[\underline{Y}_{L\Lambda} + \underline{Y}_{T\Lambda}\right]\left[\dfrac{\underline{u}_S}{\underline{u}_R}\right] \\[4pt]
\underline{i}_\Lambda \qquad \underline{Y}_\Lambda \qquad \underline{u}_\Lambda \\
\left(2n \times 2n\right)
\end{array}
\tag{11}
$$

2.1. Steady State Regime of Single Circuit EHV OHL

In order to achieve a complete analysis of an overhead line it is necessary to obtain the admittance matrix $\underline{Y}$ of the whole multiconductor system shown in Figure 3 (where S_g, S_0,…. S_L indicate the sections or ports). This involves all the elements of the line which can be represented by their admittance matrix: (by starting from the left side) the equivalent supply network matrix $\underline{Y}_{pha}$ (3×3) (see Appendix I), the load matrix $\underline{Y}_L$ (3×3) (see Appendix II), the tower matrix $\underline{Y}_{TW}$ (2×2) (see Appendix III), and, of course, the already mentioned elementary cell matrices $\underline{Y}_{\Lambda i}$. In short-circuit occurrence (Section 4), the equivalent substation impedance $\underline{Y}_{SUB}$ (3×3) and fault matrix $\underline{Y}_{fault}$ (see Appendix IV) must be considered.

On the basis of the equation which leads to the general formulation of the current vectors injected in the different ports of the system (S_g, S_0,…. S_L), it can be ascertained that the admittance matrix $\underline{Y}$ is formed by partial overlapping ("tile style") of the above mentioned matrices as shown in Figure 3b. The resulting admittance matrix $\underline{Y}$ can be of large dimensions (depending upon the ratio OHL length/Δ_ℓ) but it can be easily managed because of it is structurally sparse. Anyway, the use of the admittance frame of reference allows introducing easily local modifications of the system structure without reconstructing its entire matrix.
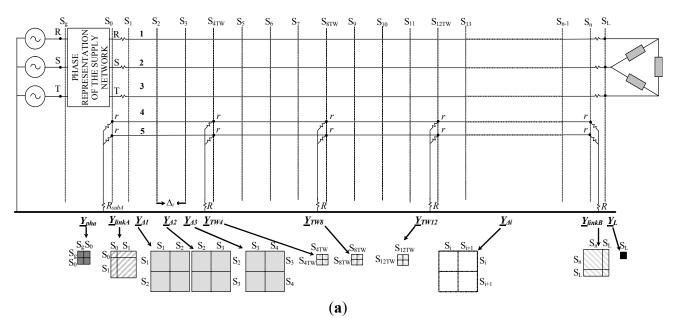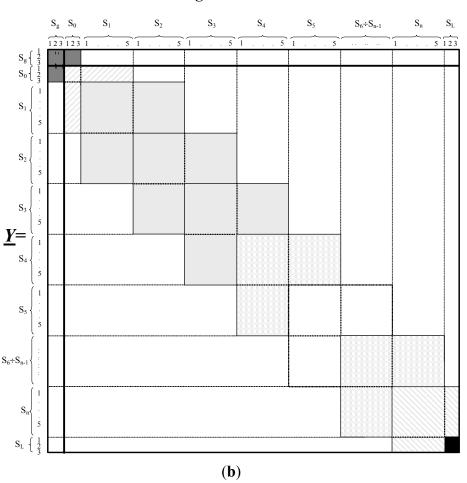
Figure 3. (**a**) Single circuit overhead line; (**b**) Structure of the matrix $\underline{Y}$.

(**a**)

Figure 3. *Cont.*

(b)

If the modification is between two sections, it is sufficient to substitute the matrix representing the modification for that existing before. If the modification is derived from a section, the matrix representing the modification must be superimposed in that section (e.g. the tower presence anywhere along the OHL). In fact, they can be represented by their admittance matrices which must be superimposed in the right location of matrix $\underline{Y}$ so to give a new total matrix $\underline{Y}_{TOT}$.

2.2. Steady State Matrix Solution of Multiconductor System

For the system of Figure 3b, the general equation $\underline{i} = \underline{Y}_{TOT}\,\underline{u}$ can be partitioned as in Figure 4. It is worth noting that only $\underline{i}_{pha}$ is a non zero current vector whereas $\underline{i}_x \equiv 0$ so that it yields:

$$\underline{i}_x \equiv 0 = \underline{Y}_3\,\underline{u}_{pha} + \underline{Y}_4\,\underline{u}_x \tag{12}$$

and thus:

$$\underline{u}_x = -\underline{Y}_4^{-1}\underline{Y}_3\,\underline{u}_{pha} \tag{13}$$

where $\underline{Y}_4$ is not singular and $\underline{u}_{pha}$ is fixed. So by knowing the subvector $\underline{u}_x$ the steady state regime of any cell, and hence of the whole multiconductor system, is completely available without iterations.
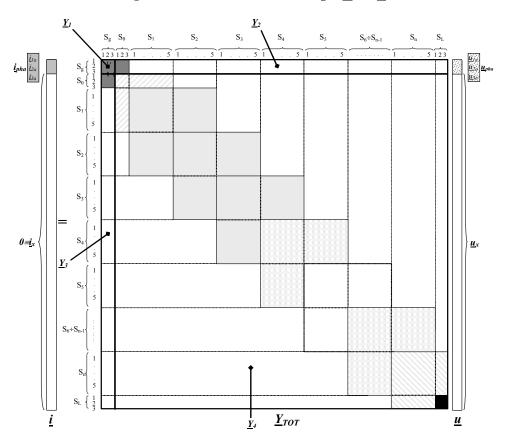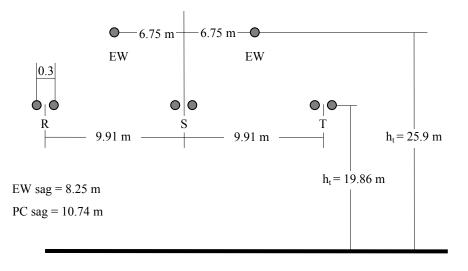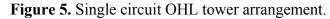
Figure 4. Partitioned matrix of $\underline{\boldsymbol{i}} = \underline{\boldsymbol{Y}}_{TOT}\,\underline{\boldsymbol{u}}$.

The inversion of $\underline{\boldsymbol{Y}}_4$ in Equation (13) could give computational drawbacks, but even if $\underline{\boldsymbol{Y}}_4$ is of great dimensions (*i.e.*, with great number of *N* cells), its inversion can benefit from the partition in submatrices [8] and the use of parallel computing.

3. Application to HV OHL on Steady State Regime

The proposed multiconductor algorithms are applied to a 275 kV 2 × 400 mm^2 single circuit aluminum conductor steel reinforced (ACSR) OHL (Figure 5), whose geometrical and electrical characteristics are reported in Table 1.

Figure 5. Single circuit OHL tower arrangement.

Table 1. OHL geometrical and electrical characteristics.

Overhead line	Symbol	Unit	Value
Voltage level	-	kV	275
Line length	-	km	55.632
Span length	-	km	0.366
Earth resistivity (assumed equal along the line)	-	Ω m	100
Symmetrical loading at receiving end	-	MW + j Mvar	$508.8 + j\ 103.32$
Substation earthing resistance	-	Ω	0.1
Tower earthing resistance (assumed equal for all the tower)	-	Ω	10
Conductor diameter (bundle conductor)	-	mm	2 sub-cond. ACSR Lynx $\Phi = 19.53$ mm
Per unit length resistance at 75° operation (50 Hz)	R	mΩ/km	96.10
Per unit length series inductance	l	mH/km	1.1051
Per unit length shunt leakance (50 Hz)	g_{av}	nS/km	44.5
Per unit length capacitance	c	μF/km	0.010215
Ampacity referred to winter rating [9]	I_a	A	545×2
Winter rating [9]	-	MVA	519.2

By means of the procedures of Section 2.2 it is possible to completely know the steady state behaviors of the electrical quantities along the line. Figure 6 shows the phase voltage behaviors along the line. There is a voltage drop which is different from phase to phase due to the asymmetrical nature of the un-transposed OHL.

Figure 6. Line-to-earth voltage magnitudes along the OHL.

The phase current magnitudes are almost constant along the line ($\cong$ 1090 A) (see Figure 7) due to the very low capacitive susceptance of OHL. The earth wire voltage along the line is almost null (see Figure 8). This is a confirmation that it is licit to use the elimination technique of grounded conductors.

It is meaningful to observe that, even in steady state regime, both the induced currents in the earth wires and the ground return current are not negligible. The earth wire induced current magnitudes along the line have an almost constant value of 96 A (see Figure 9).
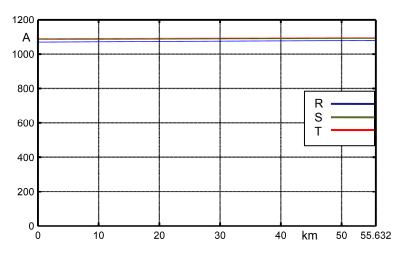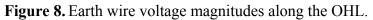
Figure 7. Phase current magnitudes along the OHL.

Figure 8. Earth wire voltage magnitudes along the OHL.
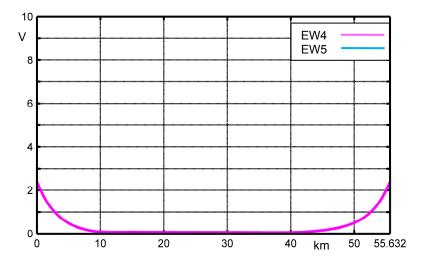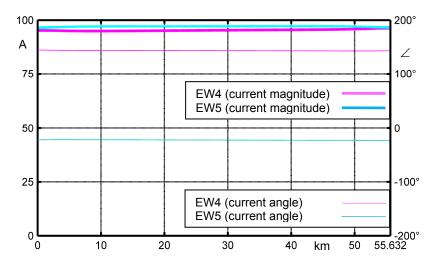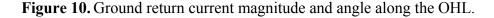

Figure 9. Earth wire current magnitudes (left axis) and angles (right axis) along the OHL.
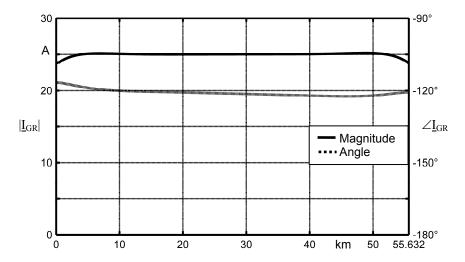

One of the most important features of MCA is that it allows directly achieving the ground return current. Since MCA can compute all the conductor current phasors in each section, I_{GR} is given by the 1st Kirchhoff's Law:

$$\underline{I}_{GR} + \sum_{x=1}^{n} \underline{I}_x \equiv 0 \Rightarrow \underline{I}_{GR} = -\sum_{x=1}^{n} \underline{I}_x \tag{14}$$

With the constant loading of Table 1 ($\underline{S}$ = 508.8 MW + j103.32 MVar), $|\underline{I}_{GR}|$ = 25 A (see Figure 10). This current could be responsible for ac metallic corrosion [10] and induced voltages on parallel metallic pipes buried in the neighborhood of OHL.

Figure 10. Ground return current magnitude and angle along the OHL.

Another important result from MCA is the possibility to compute the whole power losses which are 19.269 MW. In order to roughly validate this value, it is possible to consider a constant current in the phase conductor equal to 1090 A so that the three-phase power losses result:

$$P_{J\_PH} = 3 \cdot r \cdot L \cdot I^2 = 3 \cdot 0.0961 \cdot 55.632 \cdot 1090^2 = 19.056 \text{ MW} \tag{15}$$

To these phase conductor power losses, the insulator and corona losses must be added so that it has:

$$P_{ins+cor} = g \cdot L \cdot U^2 = 0.18722 \text{ MW} \tag{16}$$

The power losses in the earth wires are not negligible and can be computed (by considering that the induced currents are 96 A constant along the line as in Figure 9) by means of:

$$P_{EW} = 2 \cdot r_{EW} \cdot L \cdot I_{EW}^2 = 2 \cdot 0.1575 \cdot 55.632 \cdot 96^2 = 0.1615 \text{ MW} \tag{17}$$

The whole power losses are given by the sum of the three abovementioned components *i.e.*:

$$P = P_{J\_PH} + P_{ins+cor} + P_{EW} = 19.4047 \text{ MW} \tag{18}$$

which is in very good agreement with the power losses computed by MCA.

Comparison between the MCA and EMTP-RV

In this section some of the above presented MCA results are compared with the EMTP-RV results for the OHL of Section 3. The EMTP-RV electrical layout (the first and the last of four pages) is shown in Figure 11.
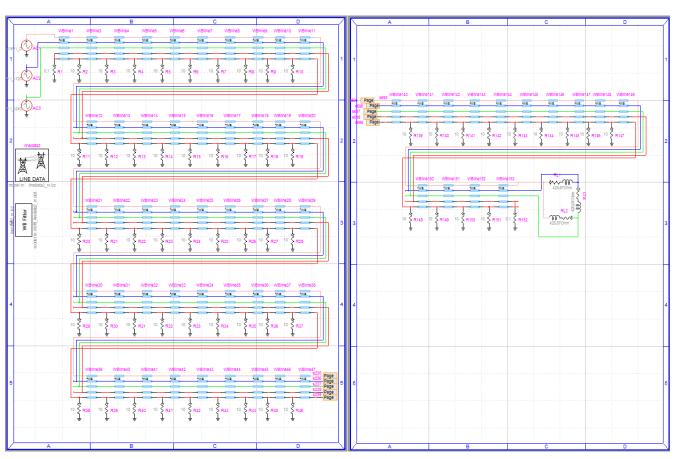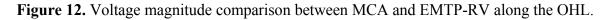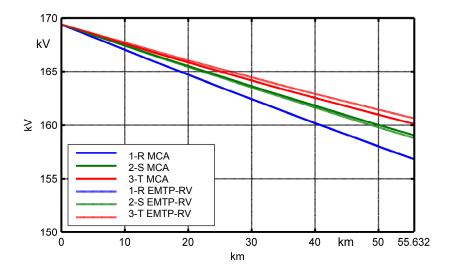
Figure 11. EMTP-RV single circuit OHL electrical layout (pages 1/4 and 4/4).

Figure 12 shows the phase voltage magnitude behavior along the single circuit OHL by means of MCA and EMTP-RV. The per cent voltage drops are reported in Table 2 where it infers that the maximum difference between the MCA and EMTP-RV is equal to 5.28%. The cpu-time in the simulation with MCA is 0.2087 s and with EMTP-RV is 0.3125 s (INTEL CORE 2 QUAD CPU@2.4 GHz, 3.25 GB RAM).

Figure 12. Voltage magnitude comparison between MCA and EMTP-RV along the OHL.

Table 2. Single circuit OHL voltage drop comparison.

Eliminate	Voltage drop [%]		
	Phase 1-R	**Phase 2-S**	**Phase 3-T**
MCA	7.4%	6.1%	5.49%
EMTP-RV	7.4%	6.26%	5.2%
Percentage difference	0.0%	2.62%	5.28%

In Table 2 "percentage difference" means:

$$100 \cdot \frac{MCA - EMTPRV}{MCA} \tag{19}$$

In Figure 13 the steady state $|\underline{I}_{GR}|$ for OHL of Section 3 is shown by using the MCA and EMTP-RV results. The maximum current difference is 1 A (4%).

Figure 13. Steady state ground return current magnitude comparison between the MCA and EMTP-RV.

4. Short-Circuit Analysis of Double-Circuit Overhead Line 400kV

In this section a double circuit OHL 400 kV 2 × 400 mm^2 ACSR, whose electrical and geometrical characteristics are reported in Table 3, has been studied on faulty regime by means of MCA (see Appendix IV). The tower arrangement is reported in Figure 14.
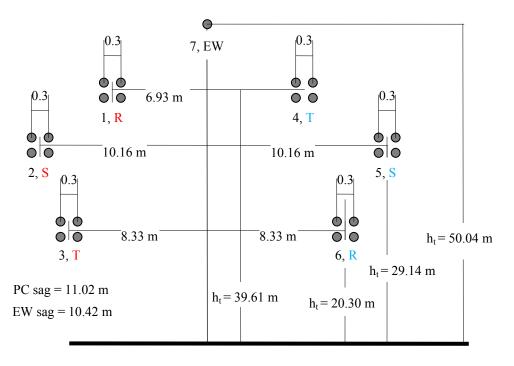
Table 3. Data assumed in the MCA for double-circuit OHL.

Overhead line	Symbol	Unit	Value
Voltage level	-	kV	400
Line length	-	km	135.42
Span length	-	km	0.366
Earth resistivity (assumed equal along the line)	-	Ω m	100
Symmetrical loading at receiving end	-	MW + j Mvar	2 × (2172.7 + j 441.2)
Substation earthing resistance	-	Ω	0.1
Tower earthing resistance(equal for all the towers)	-	Ω	10
Conductor diameter (bundle conductor)	-	mm^2	4 sub-cond. ACSR Zebra Φ = 28.62 mm

Table 3. *Cont*.

Overhead line	Symbol	Unit	Value
Per unit length resistance at 25° (50 Hz)	r	mΩ/km	8.25
Per unit length series inductance	l	mH/km	0.4218
Per unit length shunt leakance (50 Hz)	g_{av}	nS/km	33.56
Per unit length capacitance	c	µF/km	0.0266521
Ampacity referred to winter rating [11]	I_a	A	800×4
Winter rating [11] of double-circuit	MVA	-	2×2217

Figure 14. Tower characteristics of 400 kV double-circuit OHL in electric parallel with low reactance phasing.

Let us suppose the fault occurring at midline (*i.e.*, at 67.71 km from both ends) between one phase (e.g., 1R phase) and earth wire (line-to-earth short-circuit). It is worth remembering that in order to characterize the end substations it is necessary to know the fault levels (three-phase x_1, x_2 and single-phase y_1, y_2 sub-transient short circuit currents usually given by TSO) as in Figure 15.

Figure 15. Multiconductor line in short-circuit condition supplied by end substations.

Once the fault levels are known, the equivalent sequence impedances and phase impedances of each substation can be computed by means of the procedure in Appendix I, in order to create the equivalent supply network matrix. The short-circuit between a phase and the earth wire can be considered by
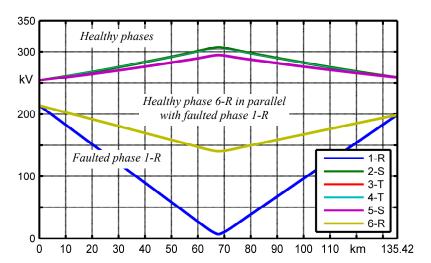
means of the matrix $\underline{\boldsymbol{Y}}_{fault}$ reported in Appendix IV. In accordance with IEC 60909-0 [12], a voltage factor must be applied to the nominal line-to-earth voltage. Since maximum currents in HV and EHV installations are considered, the voltage factor is 1.1. With regard to the resistances of the conductors, IEC-60909-0 states that, when computing the maximum currents, they have to be computed at 20 °C (cold conductors). Let us suppose the fault levels (for computation of equivalent sequence and phase impedances see Appendix IV) of Table 4. In the same table the equivalent sequence impedances have been reported.

Table 4. Data assumed in the MCA for fault levels.

Substation	Fault levels and equivalent sequence impedances
SEND.	$\left|\underline{I}_{3P}^{''}\right| = 42.62\ kA;\quad \left|\underline{I}_{1P}^{''}\right| = 43.42\ kA \mapsto \underline{Z}_1^{''} = \underline{Z}_2^{''} = j5.9604\ \Omega;\ \underline{Z}_0^{''} = j5.6310\ \Omega$
REC.	$\left|\underline{I}_{3P}^{''}\right| = 32.27\ kA;\quad \left|\underline{I}_{1P}^{''}\right| = 28.27\ kA \mapsto \underline{Z}_1^{''} = \underline{Z}_2^{''} = j7.8721\ \Omega;\ \underline{Z}_0^{''} = j11.2137\ \Omega$

Figure 16 shows the phase voltage magnitudes along the OHL. At midline the phase 1-R voltage magnitude is equal to the tower voltages (which is the same voltage of the earth wire). Also the phase 6-R of healthy circuit has a voltage drop whereas all the other phase voltage magnitudes have an overvoltage. These ones are the so called "temporary overvoltages due to earth faults" or power frequency overvoltages of relatively long duration.

Figure 17 shows the current sharing between the six phases: 6.85 kA coming from substation SEND. and 6.45 kA from substation REC. due to the different fault levels. The fault current $|\underline{I}_{IP\text{-}IR}|$ is equal to 13.304 kA whereas healthy phases (or un-faulted phases) have almost zero current. Beyond the faulted phase 1-R, the only not-negligible short circuit current flows in the phase which is in parallel with 1-R *i.e.*, 6-R (since "low reactance" phasing has been applied). The short circuit currents in all the other phases are almost zero since, according to IEC 60909-0, the shunt load admittance can be neglected so that the faulted network is at no-load.

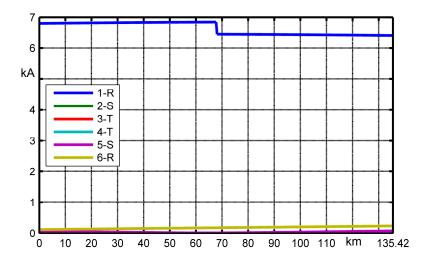**Figure 16.** Line-to-earth voltage magnitudes along the line.

Figure 17. Phase current magnitudes along the line.

The earth wire current magnitude $|\underline{I}_{EW}|$ (see Figure 18) decreases from the fault location up to a given number of spans injecting current into the earth. This number of spans, after which there is not current injection into the earth anymore, can be theoretically evaluated [7,13]. By observing Figure 18 it can be ascertained that after 8 km from the fault location the earth wire stops injecting current into the earth. Figure 19 shows the ground return current magnitudes and the angles for a midline short-circuit along the line.

It is worth noting that the exact knowledge of the ground return current behaviour results fundamental when evaluations of EMI must be assessed in a given point along the line so that the only knowledge of the sending and receiving end values $|\underline{I}_{GR}|$ are not enough.
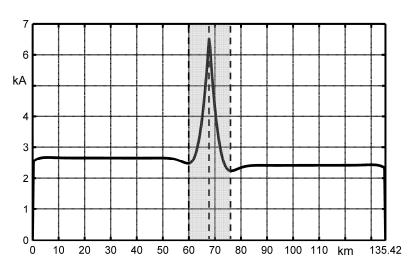
Figure 18. Earth wire current magnitude $|\underline{I}_{EW}|$ along the line in fault condition.
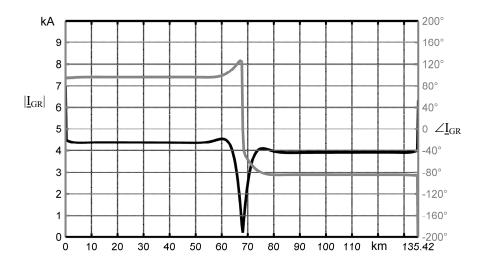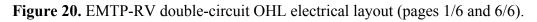
Figure 19. Ground return current magnitude $|\underline{I}_{GR}|$ and angle along the line in fault condition.

Comparison with EMTP-RV

Some of the above presented MCA results are compared with the EMTP-RV ones for the OHL of previous section whose EMTP-RV electrical layout is shown in Figure 20.
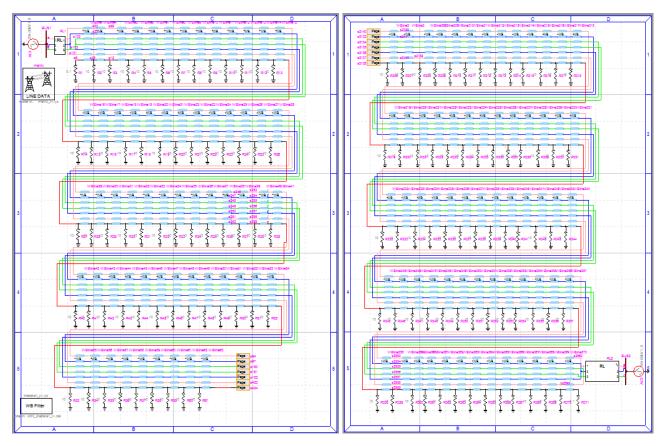
Figure 20. EMTP-RV double-circuit OHL electrical layout (pages 1/6 and 6/6).

Figure 21 shows the phase voltage magnitude behaviors along the double circuit OHL by means of MCA and EMTP-RV. The maximum percentage voltages for each phase are reported in Table 5 where the maximum value is equal to 0.95%. The cpu-time in the simulation with MCA is 3.41 s and with

EMTP-RV is 3.5 s (INTEL CORE 2 QUAD CPU@2.4 GHz, 3.25 GB RAM). $|\underline{I}_{GR}|$ comparison is shown in Figure 22. The maximum difference between the MCA and EMTP-RV ground current magnitude is 77 A (−1.9%). In conclusion, the agreement between MCA and EMTP-RV is extremely good.

Figure 21. Line-to-earth voltage magnitude comparison between the MCA and EMTP-RV under phase-to-earth short circuit in a double-circuit OHL.
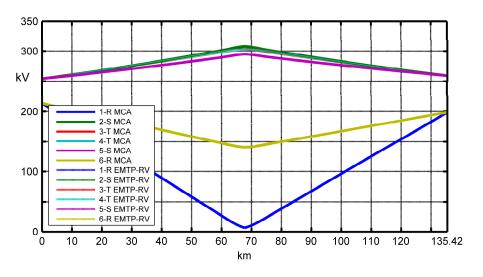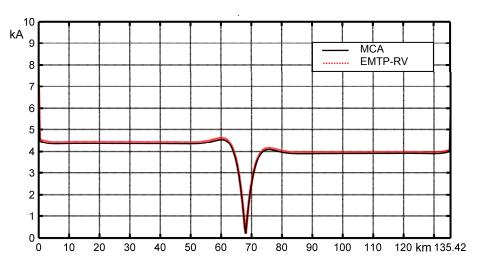

Table 5. Double-circuit line maximum voltage magnitude comparison.

Eliminate	Max. faulted circuit voltage magnitudes [kV]			Max. healthy circuit voltage magnitudes [kV]		
	Phase 1-R (faulted phase)	Phase 2-S	Phase 3-T	Phase 6-R	Phase 5-S	Phase 4-T
MCA	6,68	307,7	304,6	140,4	294,8	303,8
EMTP-RV	6,74	308,8	301,7	141,4	295,3	301,9
Percentage difference	−0.9%	−0.36%	0.95%	−0.71%	0.16%	0.62%

Figure 22. Ground return current comparison between the MCA and EMTP-RV under line-to-earth short circuit in a double-circuit OHL.

5. Conclusions

MCA has already had a great number of successful applications to multi-phase asymmetrical systems [1–3]. In this paper, it has been applied to overhead lines with bundled phase conductors and one or more earth wires. The steady state regime of a typical un-transposed HV OHL has highlighted that there is a not negligible ground return current which may lead to electromagnetic interferences and ac corrosion issues. In faulty analysis, the behaviour of ground return current can be directly achieved so to recognize the number of spans after which the injection of currents in the ground terminates and the ground return current becomes constant. MCA is also extremely useful to evaluate the rise of earth potential at substation sites. Further researches are needed in order to validate the screening factor approach by means of MCA tool. Comparisons with EMTP-RV commercial software has demonstrated a very good agreement.

Appendix I. Equivalent Supply Network Matrix

In the study of multiconductor steady state regimes the following positive sequence voltage vector must be directly applied:

$$\underline{u}_{ph} = \begin{bmatrix} 1 \\ \alpha^2 \\ \alpha \end{bmatrix} \cdot \frac{U_N}{\sqrt{3}} \quad \alpha = e^{j\frac{2}{3}\pi} \tag{A1}$$

(e.g., for $U_N = 400$ kV $\rightarrow U_N / \sqrt{3} \cong 230$ kV) and for the study of the multiconductor no-load energization, also a phase model of the supply network must be introduced by means of the matrix $\underline{Z}_{pha}$.

By assuming a perfectly symmetric structure of the three phase supply network it can be fully characterized by the corresponding zero, positive and negative longitudinal impedances derived from the sub-transient short-circuit currents (single-phase and three-phase ones). The corresponding phase matrix $\underline{Z}_{pha}$ can be obtained by means of the Fortescue's transformations:

$$\underline{u}_S = \underline{F} \cdot \underline{u}_{pha} \qquad \underline{i}_S = \underline{F} \cdot \underline{i}_{pha} \tag{A2}$$

$$\underline{u}_{pha} = \underline{F}^{-1} \cdot \underline{u}_S \qquad \underline{i}_{pha} = \underline{F}^{-1} \cdot \underline{i}_S \tag{A3}$$

If a passive symmetric tripole is considered the following diagonal matrix relations can be formed

$$\begin{array}{c} \boxed{\begin{array}{c} \underline{U}_{R0} \\ \underline{U}_{R1} \\ \underline{U}_{R2} \end{array}} = \boxed{\begin{array}{ccc} \underline{Z}_0 & 0 & 0 \\ 0 & \underline{Z}_1 & 0 \\ 0 & 0 & \underline{Z}_2 \end{array}} \boxed{\begin{array}{c} \underline{i}_{R0} \\ \underline{i}_{R1} \\ \underline{i}_{R2} \end{array}} \\ \underline{U}_S \qquad\qquad \underline{Z}_S \qquad\qquad \underline{i}_S \end{array} \tag{A4}$$

By using Equations (A.2,A.3) and by arranging Equation (A.4), it is possible to compute the phase impedance matrix $\underline{Z}_{pha}$ from the sequence impedance matrix $\underline{Z}_S$, as in Equation (A.8):

$$F\underline{u}_{pha} = \underline{Z}_S \underline{i}_S \tag{A5}$$

$$\underline{u}_{pha} = \underline{F}^{-1}\underline{Z}_S \underline{i}_S \tag{A6}$$

$$\underline{u}_{pha} = \underline{F}^{-1}\underline{Z}_S \underline{F}\underline{i}_{pha} = \underline{Z}_{pha}\underline{i}_{pha} \tag{A7}$$

$$\underline{Z}_{pha} = \underline{F}^{-1}\underline{Z}_S \underline{F} \tag{A8}$$

By following the same criteria used for the longitudinal block **L** of Section 2 it is possible (see Figure A1) to achieve for the block **A** the matrix $\underline{Y}_{pha}$ which characterizes the power supply in the sub-transient regimes.

Figure A1. (**a**) Supply network modelling (sequence); (**b**) Supply network modelling (Multiconductor).

If faulty conditions are considered, this model must be applied at both ends in order to take in account the two end substations (with their sub-transient fault levels).
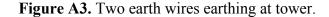
Figure A2. Model of complex load at receiving end.
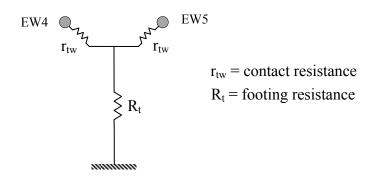
Appendix II. Equivalent Load Matrix

In order to model a complex power loading at receiving-end, a three-phase balanced static load can be considered as in Figure A2. The value of $\underline{y}_L$ is calculated so that the three admittances absorb, once applied the rated positive sequence voltage *u*, the rated receiving-end three-phase complex power $\underline{S}_L$:

$$\underline{y}_L = \frac{\underline{S}_L^*}{3 \cdot u^2} \tag{A9}$$

Appendix III. Earthing Technique

The earthing of own two earth wires (see Figure A3) in correspondence of the tower must be considered with its admittance matrix $\underline{Y}_{TW}$ (2 × 2). This matrix presents different composition depending on the earth wire earthing technique.
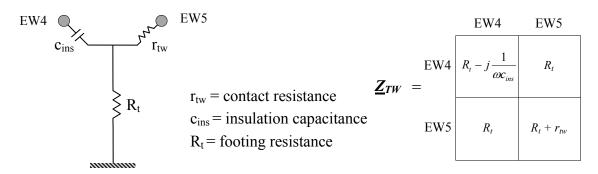
Figure A3. Two earth wires earthing at tower.

The formation of $\underline{Y}_{TW}$ is rather simple and involves the inversion of nodal impedance matrix *i.e.*,:

$$\underline{Y}_{TW} = \underline{Z}_{TW}^{-1} \tag{A10}$$

The "contact resistance" r_{tw} accounts for the resistance due to the tower presence and can be set to a very small value *i.e.*, $r_{tw} = 10^{-3}$ Ω. Differently R_t can range between about 5 and 20 Ω.
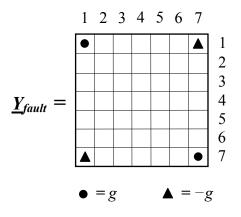
Figure A4. EW4 insulation from tower.

In some transmission grids, the EWs are insulated from the tower. This can be made in order to supply discharge lamps [14] which warn the presence of tower itself or to zero the EW power losses (usually for very long OHLs as in Brazil). For example, if EW4 is insulated from the tower (see Figure A4), the suitable admittance must be considered.

Appendix IV. Short-Circuit Analysis

The short-circuit, for OHL in Section 4, between phase 1-R and earth wire can be easily considered by constructing the following matrix, where numbers 1, 2, 3, ... 6 are the phase conductors and number 7 is the earth wire (Figure A5):

Figure A5. Admittance matrix representing a line-to-earth short circuit.

where g must account for the short-circuit conductance (e.g., 1 kS). The matrix $\underline{Y}_{fault}$ must be superimposed in $\underline{Y}_{TOT}$ in the location corresponding to the faulty section. By means of this matrix technique other types of fault can be easily assessed e.g. phase interruptions, multiple dead and not short-circuits. By considering the fault levels, the sequence impedances for each substation can be computed by the well-known formulae:

$$\underline{I}''_{3P} = 1.1 \cdot \frac{\underline{E}_{PV}}{\underline{Z}''_1} \tag{A.11}$$

$$\underline{I}''_{1P} = 1.1 \cdot \frac{3\underline{E}_{PV}}{\underline{Z}''_1 + \underline{Z}_2 + \underline{Z}_0} \tag{A.12}$$

By solving the Equations (A11,A12) it yields:

$$\underline{Z}''_1 = \underline{Z}_2 = 1.1 \cdot \frac{\underline{E}_{PV}}{\underline{I}''_{3P}} \tag{A.13}$$

$$\underline{Z}_0 = 1.1 \cdot \underline{E}_{PV} \cdot \left(\frac{3}{\underline{I}''_{1P}} - \frac{2}{\underline{I}''_{3P}} \right). \tag{A.14}$$

Once the diagonal sequence matrix $\underline{Z}_S$ has been computed, it is easy to compute the phase matrix $\underline{Z}_{pha}$ by means of Fortescue matrix $\underline{F}$ (as clearly shown in Appendix I).

Once the $\underline{Y}_{TOT}$ has been computed the faulty regime can be evaluated with a suitable partition of it as in Figure A6.
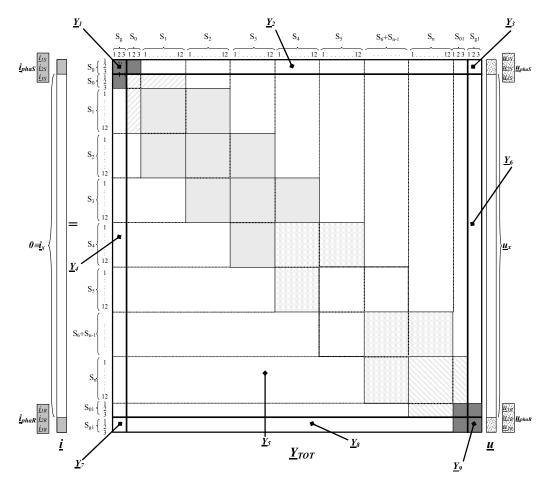
Figure A6. Partitioned matrix of $\underline{i} = \underline{Y}_{TOT}\underline{u}$ in short-circuit occurrence.

The study of short-circuit leads to the following equations:

$$\underline{i}_{phaS} = \underline{Y}_1 \underline{u}_{phaS} + \underline{Y}_2 \underline{u}_x + \underline{Y}_3 \underline{u}_{phaR} \tag{A15}$$

$$0 = \underline{Y}_4 \underline{u}_{phaS} + \underline{Y}_5 \underline{u}_x + \underline{Y}_6 \underline{u}_{phaR} \tag{A16}$$

$$\underline{i}_{phaR} = \underline{Y}_7 \underline{u}_{phaS} + \underline{Y}_8 \underline{u}_x + \underline{Y}_9 \underline{u}_{phaR} \tag{A17}$$

where the vector $\underline{i}_x$ is null (see Figure A6). From Equation (A16), it is rather immediate to obtain the unknown vector $\underline{u}_x$:

$$\underline{u}_x = -\underline{Y}_5^{-1} \cdot \left(\underline{Y}_4 \underline{u}_{phaS} + \underline{Y}_6 \underline{u}_{phaR} \right) \tag{A18}$$

Once again, if $\underline{Y}_5$ is of great dimensions, its inversion can benefit from the partition techniques and parallel computing.

Acknowledgments

References

1. Benato, R.; Paolucci, A. *EHV AC Underground Electrical Power. Performance and Planning*; Springer: Berlin, Germany, 2010.
2. Benato, R. Multiconductor analysis of underground power transmission systems: EHV AC Cables. *Electr. Power Syst. Res*. **2009**, *79*, 27–38.
3. Benato, R.; Brunello, P.; Carlini, E.M.; di Mario, C.; Fellin, L.; Knollseisen, G.; Laußegger, M.; Muhr, M.; Paolucci, A.; Stroppa, W.; Wörle, H.; Woschitz, R. Italy-Austria GIL in the new planned railway galleries Fortezza-Innsbruck under Brenner Pass. *Elektrotech. Informationstechnik* **2006**, *123*, 551–558.
4. International Telecommunication Union. *Directives Concerning the Protection of Telecommunication Lines against Harmful Effects from Electric Power and Electrified Railway Lines*; ITU: Geneva, Switzerland, 1989.
5. Carson, J.R. Wave propagation in overhead wires with ground return. *Bell Syst. Tech. J.* **1926**, *5*, 539–554.
6. Dommel, H.W. *Electromagnetic Transients Program Reference Manual (EMTP Theory Book)*; Bonneville Power Administration: Portland, OR, USA, 1986.
7. Nasser, D.; Tleis, A. *Power Systems Modelling and Fault Analysis: Theory and Practice*; Newnes: London, UK, 2008.
8. Braae, R. *Matrix Algebra for Electrical Engineers*; Pitman & Sons: London, UK, 1963.
9. Booth, E.S.; Clark, D.; Egginton, J.L.; Forrest, J.S. The 400 kV grid system for England and Wales. *Proc. IEE Part A Power Eng.* **1962**, *109*, 493–511.
10. *AC Corrosion on Metallic Pipelines due to Interference from AC Power Lines—Phenomenon, Modelling and Countermeasures*; Cigré Technical Brochure # 290; Cigré: Paris, France, 2006.
11. British Electricity International. *Modern Power Station Practice, EHV Transmission*; Permagon: Oxford, UK, 1991.
12. International Electrotechnical Commission. *Short-Circuit in Three-Phase A.C. Systems. Part 1: Calculations of Current*, 1st ed.; IEC 60909-0; International Electrotechnical Commission: Geneva, Switzerland, 2001.
13. Paolucci, A. *Lezioni di Trasmissione Dell'energia Elettrica* ; CLEUP: Padova, Italy, 1998.
14. Benato, R.; Paolucci, A.; Turri, R. Insulated Ground wire capacitive currents for tower discharge warning lamp supplying. *Electr. Power Syst. Res.* **2004**, *71*, 211–221.